Archives of Materials Science and Engineering

Volume 28
Issue 7
July 2007
Pages 417-420

International Scientific Journal
published monthly as the organ of
the Committee of Materials Science
of the Polish Academy of Sciences

# Modelling of transport phenomena in gas tungsten arc welding

**A. Farzadi*, S. Serajzadeh, A.H. Kokabi**
Materials Science and Engineering Department, Sharif University of Technology, Azadi Ave., Tehran, Iran
* Corresponding author: E-mail address: farzadi@mehr.sharif.edu

Received 20.04.2007; published in revised form 01.07.2007

**ABSTRACT**

**Purpose:** Since numerical heat transfer and fluid flow models have provided significant insight into welding process and welded materials that could not been achieved otherwise, there has been an important interest in the quantitative representation of transport phenomena in the weld pool. On the other hand, the temperature and velocity distributions of the molten metal as well as the cooling rate after welding operation affect the weld geometry, the microstructure, and the mechanical properties of weld zone. This work demonstrates that the application of numerical transport phenomena can significantly add to the quantitative knowledge in welding and help the welding community in solving practical problems.

**Design/methodology/approach:** The temperature and velocity fields are simulated using the solution of the equations of conversation of mass, energy and momentum in three-dimension and under steady-state heat transfer and fluid flow conditions.

**Findings:** The weld pool geometry and various solidification parameters were calculated. The calculated weld pool geometries were in good agreement with the ones obtained using the experiments. The solidification parameters of G and G/R are determined. It is found that as the welding speed increases, the value of G/R at the weld pool centerline decreases.

**Research limitations/implications:** Welding process used is this study is gas tungsten arc (GTA) welding and base metal is commercial pure aluminum. This model can be investigated to simulate other materials and welding processes. Also the results of this study such as the temperature field can be used in the simulation of microstructure, mechanical properties, etc of welding zone.

**Originality/value:** In this research the solidification parameters of G, R and G/R can be used for prediction of the solidification morphology and the scale of the solidification structure.

**Keywords: Computational mechanics; GTA welding; Transport phenomena; Commercial pure aluminium**

**METHODOLOGY OF RESEARCH, ANALYSIS AND MODELLING**

## 1. Introduction

In first attempts, significant progress has been made in the solution of the equations of conservation of mass, momentum and energy in fusion welding with a stationary heat source [1]. However, in practice, the heat source moves with a certain velocity. Thus, several investigations of fluid flow and heat transfer in welding with moving heat source have been reported [2, 3]. The three dimensional (3D) comprehensive numerical heat transfer and fluid flow model used in the calculations has been extensively validated for the welding of steels [4-7], aluminum alloys (5182 and Al-Cu) [8, 9], and titanium alloys [10]. However, most of these studies were concerned with iron and its alloys while the heat transfer and fluid flow in the commercial pure aluminum have not received much attention in the literature.

Numerical calculations of heat transfer and fluid flow in welding have enabled accurate quantitative calculations of thermal cycles and fusion zone geometry [2, 11]. Capabilities to quantitatively understand geometry, composition and structure of welds in simple systems have provided hope that one day welding engineers may be able to use numerical models to tailor weldment characteristics according to specifications. In reality, the numerical heat transfer and fluid flow codes for fusion welding have so far been used mostly as a research tool [4, 5] rather than as a tool for design and manufacturing in the industry but application of commercial code such as FLUENT can aid to reach this goal.

In this study, the heat transfer and fluid flow GTA welds of commercial pure aluminum were simulated using a well-tested, three-dimensional, steady state, numerical heat transfer and fluid flow model. The model was applied to understand the temperature field and the weld dimensions for various GTA welding conditions. For the accuracy of the calculation, a very fine grid system was used. Verification of the model was performed through comparing the calculated results with metallographic weld cross sections. Several important solidification parameters, including solidification rate (R) and temperature gradient (G) at the weld centerline, were calculated. These parameters may be used for determination of the solidification morphology and the scale of the solidification substructure.

## 2. Mathematical formulation

An incompressible laminar and Newtonian liquid flow is assumed in the weld pool. The density variation in the calculation domain is ignored except for the calculation of the buoyancy force following Bossinesq's approximation. Electromagnetic, surface tension, and buoyancy driving forces were considered for the calculation of weld pool convection. The weld pool boundary was traced using an enthalpy-porosity technique in a fixed Cartesian coordinate system.

### 2.1. Governing equations

Using the assumptions stated above, the circulation of liquid metal in the weld pool can be represented by the following linear momentum conservation equation for the jth direction:

$$\rho\frac{\partial(u_i u_j)}{\partial x_i}=-\frac{\partial P}{\partial x_j}+\frac{\partial}{\partial x_i}(\mu\frac{\partial u_j}{\partial x_i})+\frac{\partial}{\partial x_j}(\mu\frac{\partial u_j}{\partial x_j}) + \rho U\frac{\partial u_i}{\partial x_i}-C\left(\frac{(1-f_L)^2}{f_L^3+B}\right)u_j+Sb_j+Se_j \quad (1)$$

where ρ is density, $x_i$ is the distance along the i=1, 2, and 3 directions, $u_j$ is the velocity component along the j direction, μ is the viscosity, p is the pressure, $f_L$ is the liquid fraction, B is a constant introduced to avoid division by zero, C is a constant that considers mushy zone morphology, U is the welding speed along the positive x direction, and $Sb_j$ and $Se_j$ present the electromagnetic and buoyancy source terms, respectively. In Eq. (1), the first term on the right-hand side is the pressure gradient. The second term is the viscosity arising from casting the momentum equation into a general form. The fifth term describes the frictional dissipation in the mushy zone according to the Carman-Kozeny equation for flow through a porous media. The calculation of the electromagnetic and buoyancy source terms is expressed in the literatures [2, 12].

The pressure field was obtained by solving following continuity equation simultaneously with the momentum equation:

$$\frac{\partial(\rho u_i)}{\partial x_i}=0 \quad (2)$$

The total enthalpy H is represented by a sum of sensible heat h and latent heat content ΔH, i.e., H = h + ΔH, where $h=\int C_P\,dT$, $C_P$ is the specific heat, T is the temperature, $\Delta H = f_L L$, L is the latent heat of fusion, and the liquid fraction $f_L$ is assumed to vary linearly with temperature in the mushy zone:

$$f_L=\begin{cases}1, T>T_L\\ \dfrac{T-T_S}{T_L-T_S}, T_S\le T\le T_L\\ 0, T<T_S\end{cases} \quad (3)$$

where $T_L$ and $T_S$ are the liquidus and the solidus temperatures, respectively. The thermal energy transport in the weld workpiece can be expressed by the following modified energy equation:

$$\rho\frac{\partial(u_i h)}{\partial x_i}=\frac{\partial}{\partial x_i}\left(\frac{k}{C_p}\frac{\partial h}{\partial x_i}\right)-\rho\frac{\partial(u_i\Delta H)}{\partial x_i}+ \rho U\frac{\partial\Delta H}{\partial x_i}+\rho U\frac{\partial h}{\partial x_i} \quad (4)$$

where k is the thermal conductivity.

### 2.2. Solution procedure

A 3D Cartesian coordinate system is used in the calculation, while only half of the workpiece is considered since the weld is symmetrical about the weld center line. These boundary conditions are further discussed as follows.

The top surface is assumed to be flat and subject to shear stress due to Marangoni force. Also $u_z$ is defined to be zero at the surface. The heat flux on the top surface is given as

$$k\frac{\partial T}{\partial x_3}\Big|_{top}=\frac{fQ\eta}{r_b^2}\exp\left(-\frac{f(x^2+y^2)}{r_b^2}\right)-h(T-T_a) \quad (5)$$

where $r_b$ is the heat distribution parameter, f is the power distribution factor, Q is the total arc power, η is the power efficiency, h is the heat transfer coefficient, and $T_a$ is the ambient temperature.

At the symmetric surface, $u_y$ and the normal gradients of $u_x$ and $u_z$ are taken as zero. In addition, the gradient of enthalpy, dh/dy , is zero.

At all other surfaces, the heat losses by convection and the velocities are set to be zero.

The detailed method of discretizing the governing equations is available in the literature [2, 15]. The governing equations are discretized using the control volume method [13], where the computational domain is divided into small rectangular control volumes. A staggered grid is used to store the velocity

components. To numerically solve the governing equations with the associated source terms, a general computational fluid dynamics (CFD) computer program, FLUENT code was used. The material properties employed in the calculation of fluid flow and heat transfer are summarized in Table 1 [4]. The velocity-pressure coupling in the discretized momentum equations is handled using SIMPLE algorithm at the each iteration [15, 16].

Accurate calculation of weld temperature and velocity fields, and the temperature gradients requires the use of a very fine grid system. A typical grid system used in the present study contained 143x73x50 grid points, and the corresponding computational domain had dimensions of 100 mm in length, 45 mm in width, and 5 mm in depth. Spatially non uniform grids were used for maximum resolution of variables. A finer grid spacing was used near the heat source. The minimum grid spacings along the x and z directions were about 50 and 20μm, respectively.

In the present study, the convergence was reached when $R \leq 10^{-4}$ for the energy equation and $R \leq 10^{-3}$ for the momentum equations.

Table 1.
Physical properties of commercial pure aluminum used in the calculations [14]

| Physical Property | Value |
|---|---|
| Liquid temperature, $T_L$ (K) | 930 |
| Solid temperature, $T_S$ (K) | 916 |
| Density of liquid metal, ρ(kg/m3) | 2700 |
| Viscosity of liquid, μ(kg/m s) | 0.0014 |
| Thermal conductivity of solid, $k_S$ (J/m s K) | 222 |
| Thermal conductivity of liquid, $k_L$ (J/m s K) | 108 |
| Specific heat of solid, $C_{PS}$ (J/kg K) | 904 |
| Specific heat of liquid, $C_{PL}$ (J/kg K) | 904 |
| Latent heat of melting, ΔH (J/kg) | $3.95 \times 10^5$ |
| Temperature coefficient of surface tension, $d\gamma / dT$ (N/m K) | $-0.152 \times 10^{-3}$ |
| Coefficient of thermal expansion, β ($K^{-1}$) | $2.55 \times 10^{-5}$ |
| Magnetic permeability, $\mu_m$ ($N/A^2$) | $1.26 \times 10^{-6}$ |

### 2.3. Experimental procedure

Commercial pure aluminum plate with the thickness of 5 mm was used in this investigation. The composition of the as-received bar was (by wt%): 0.08 Si, 0.29 Fe, 0.005 Cu, 0.002 Mn, 0.002 Mg, 0.06 Zn, 0.003 Ti, 0.001 Cr, and 0.002 Ni. The welding electrode was made of W-2%Th measuring 2.4 mm in diameter. High Purity (99.99%) argon was used as welding gas. In welding experiments, the arc current, the arc voltage and welding speed were 110 A, 15 V and 2.7 mm/s, respectively.

## 3. Results and discussion

### 3.1. Temperature and velocity fields

The experimentally determined weld pool cross sections are compared with the corresponding calculated geometries in Figure 1. It is observed that the computed weld pool geometry and dimensions agree well with the experimental results. In these figures, the mushy zone, i.e. the solid and liquid two phase region is presented with the distinct color. In the present study, the mushy zone is determined as the region having temperature between the solidus (916 K) and liquidus (930 K) isotherms.

Figure 2 shows the computed 3D temperature and velocity fields for a weld pool made by welding conditions presented in section 2.3. For clarify; only a half of weld is shown. The liquid metal motion in the weld pool is driven mainly by the surface tension and electromagnetic forces, and to a much lesser extent, by the buoyancy force. The relative importance of these driving forces is quantitatively examined in a subsequent section. Because the temperature coefficient of surface tension $d\gamma / dT$ has a negative value, the surface tension force drives the liquid metal from the center to the periphery at the top surface of the weld pool. The peak temperature and maximum velocity are 1746 K and 1.445 m/s, respectively.

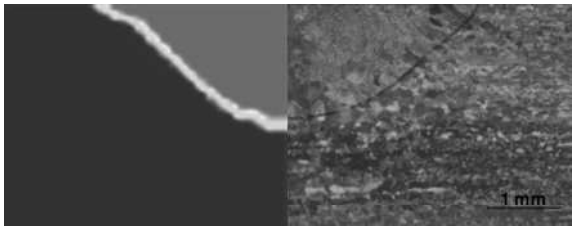


Fig. 1. Experimental and calculated weld pool cross sections for GTA welds. Welding condition was expressed in Sec. 2.3

### 3.2. Solidification

The average temperature gradient, $\overline{G}_a$, of the weld pool along a given plane is defined as

$$\overline{G}_a = \frac{T_P - T_S}{d} \tag{6}$$

where $T_P$ is the peak temperature, $T_S$ is the solidus temperature, and d is the distance between the location of peak temperature and boundary at the weld pool centerline.

The temperature gradient and the solidification rate are important in the combined forms G/R as they influence the solidification morphology and the scale of the solidification substructure, respectively. When the value of G/R increases, the interface morphology changes from equiaxed-dendritic, to cellular-dendritic, to cellular grains [17]. Figure 3 shows the temperature gradient G and G/R at the weld centerline for different welding speed. It is shown that with the increase in welding speed the temperature gradient decreases and the value of G/R decreases at the weld pool centerline. Thus the solidification structure of fusion zone would be affected by welding speed.

## 4. Conclusions

The temperature and velocity fields, weld pool size, and several solidification parameters during GTA welding of commercial pure aluminum were simulated using a comprehensive three-dimensional

heat transfer and fluid flow model. The major conclusions can be made from investigation are as follows:

(1) The geometry of fusion zone predicted from the three-dimensional steady state heat transfer and fluid flow model using FLUENT code are in a good agreement with the corresponding experimental results.
(2) The value of G/R at the weld pool centerline is shown to decrease with the increase in welding speed.

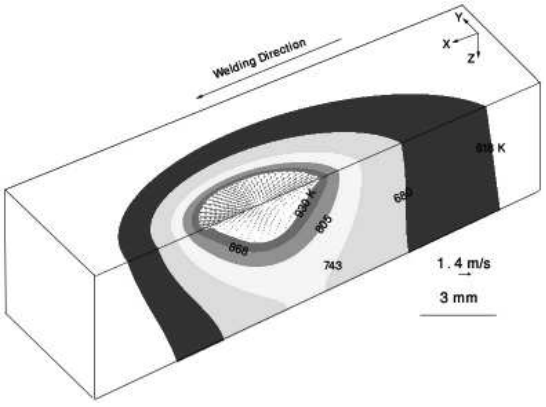


Fig. 2. Calculated temperature and velocity fields in three dimensions. Welding condition was presented in Sec. 2.3

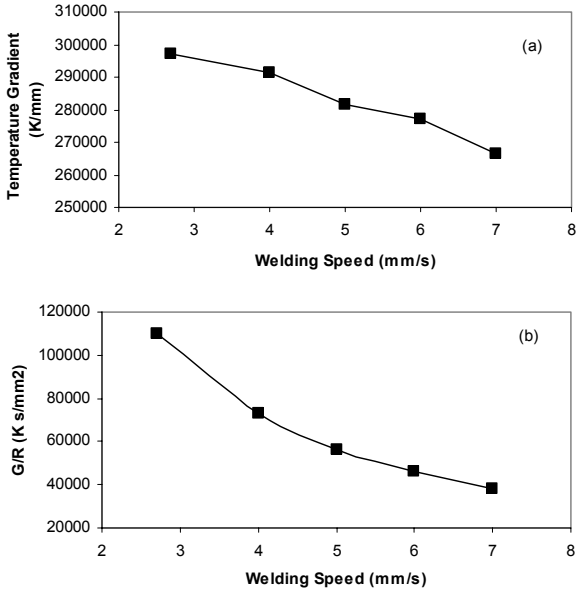


Fig. 3. Calculated values of (a) G, (b) GR and (c) G/R at the weld pool centerline at different welding speed

## References


[1] S. Kou, D.K. Sun, Fluid flow and weld penetration in stationary arc welds, Metallurgical Transaction A 16A (1985) 203-213.
[2] K. Mundra, T. DebRoy, K.M. Kelkar, Numerical prediction of fluid flow and heat transfer in welding with a moving heat source, Numerical Heat Transfer, Part A 29 (1996) 115-129.
[3] S. Kou, Y.H. Wang, Computer simulation of convection in moving arc weld pools, Metallurgical Transaction A 17A (1986) 2271-2277.
[4] W. Zhang, G.G. Roy, J.W. Elmer, T. DebRoy, Modeling of heat transfer and fluid flow during gas tungsten arc spot welding of low carbon steel, Journal of Applied Physics 93 (2003) 3022-3033.
[5] X. He, P.W. Fuerschbach, T. DebRoy, Heat transfer and fluid flow during laser welding of 304 stainless steel, Journal of Physics D: Applied Physics 36 (3002) 1388-1398.
[6] A. De, T. DebRoy, Probing unknown welding parameters from convective heat transfer calculation and multivariable optimization, Journal of Physics D: Applied Physics 37 (2004) 140-150.
[7] X. He, J.W. Elmer, T. DebRoy, Heat transfer and fluid flow in Laser microwelding, Journal of Applied Physics 97 (2005) 1-9.
[8] H. Zhao, T. DebRoy, Weld metal composition change during conduction mode laser welding of aluminum alloy 5182, Metallurgical Transaction B 32B (2001) 163-172.
[9] S. Mishra, S. Chakraborty, T. DebRoy, Probing liquation cracking and solidification trough modeling of momentum, heat, and solute transport during welding of aluminum alloys, Journal of Applied Physics 97 (2005) (1-9).
[10] Z. Yang, S. Sista, J.W. Elmer, T. DebRoy, Three dimensional Monte Carlo simulation of grain growth during GTA welding of titanium, Acta Materialia 48 (2000) 4813-4825.
[11] J.W. Elmer, T.A. Zhang, B. Wood, T. DebRoy, Kinetic modeling of phase transformations in the occurring in the HAZ of C-Mn steel welds based on direct observations, Acta Materialia 51 (2003) 3333-3349.
[12] A. Kumar, T. DebRoy, Calculation of three-dimensional electromagnetic force field during arc welding, Journal of Applied Physics 94 (2003) 1267-1277.
[13] S.V. Patankar, Numerical Heat Transfer and Fluid Flow. Hemispher, Washington-New York-London, 1980.
[14] J.E. Hatch, Aluminum: Properties and Physical Metallurgy. Metals Park, Ohio: American Society for Metals, 1984.
[15] C.-P. Hong, Computer Modeling of Heat and Fluid Flow in Materials Processing. Institute of Physics Publishing, Bristol and Philadelphia, 2004.
[16] FLUENT Inc., FLUENT User's Guide. 2001.
[17] S. Kou, Welding Metallurgy. Second Edition, Wiley Interscience, New Jersey, 2003.